Isosteric Heat of Argon Adsorbed on Single-Walled Carbon Nanotubes Prepared by Laser Ablation

Vaiva Krungleviciute,[†] Luke Heroux,[†] Aldo D. Migone,*[,†] Christopher T. Kingston,[‡] and Benoit Simard[‡]

Department of Physics, Southern Illinois University, Carbondale, Illinois 62901-4401, and Steacie Institute for Molecular Sciences, National Research Council, 100 Sussex Drive, Ottawa, Ontario K1A 0R6, Canada

Received: December 16, 2004; In Final Form: March 18, 2005

We have measured 21 adsorption isotherms for argon on single-walled carbon nanotubes produced by laser ablation. We explored temperatures between 40 and 153 K to obtain the coverage dependence of the isosteric heat of adsorption for films in the first and second layers. Our data are compared to results obtained in computer simulation studies and to data obtained in previous experimental investigations of this system.

1. Introduction

Single-walled carbon nanotubes (SWNTs), because of their unique structure and characteristics, have captured the interest and the imagination of researchers in fundamental and applied materials science ever since they were discovered in 1993 by Iijima.[1] After they are produced, owing to van der Waals attractions between them, SWNTs assemble into bundles consisting of between tens to a few hundred of individual tubes, packed in a hexagonal array.[2]

The study of gas adsorption on SWNT bundles is an area that continues to attract the interest of theorists, experimentalists, and computer simulationists alike. One of the questions upon which much of the research activity has focused is that of determining where on the nanotube bundles is a given atom or molecule of gas adsorbing. The isosteric heat measurements, which we report below, when combined with the results of computer simulations, provide a useful approach to address this important question.

The first theoretical model for the SWNT bundles used in simulations to study adsorption described the bundles as defect-free, hexagonal arrays of rigid tubes, all of the same diameter ("homogeneous bundle").[3,4] A homogeneous bundle has four groups of sites that may, potentially, be available for adsorption. These are the outer surface of individual tubes located on the periphery of the bundles (outer sites), the convex valleys between two adjacent tubes on the periphery of the bundle (grooves), the open spaces at the interior of the bundles that are left in the region where three tubes come close together (interstitial channels (ICs)), and if the tube ends are opened, the space in the interior of the individual tubes.[3,4] In the homogeneous bundle model, all of the ICs are of the same size, and they are too small to accommodate any but the smallest adsorbates (^{4}He, H_2, and Ne) within them. Whether adsorption occurs or not in the ICs for any species is a matter of some controversy.[3,5−10]

Recently, two other nanotube bundle models have been proposed. In one of them, the heterogeneous model, the bundles consist of rigid tubes of different diameters.[11] Diameter heterogeneity always results in the appearance of packing defects. In this model, these defects result in a small number of large-diameter ICs. The other model, the heterogeneous deformable bundle,[12] consists of deformable tubes of different diameters. There are no large-diameter ICs present in the heterogeneous deformable bundle model because in it the tubes deform to occupy most of the open space available as a result of packing defects.

Experimental researchers have used different techniques (X-ray[1,13,14,16] and neutron[17] diffraction, Raman scattering,[13−18] electron microscopy,[1,13−16,19] and scanning tunneling microscopy and spectroscopy[16,20]) to obtain information, among other things, on the makeup of the bundles. The problem of determining the distribution of nanotube diameters within a bundle is a difficult one (for example, ref 16 notes that determination of the tube diameter from TEM images, a commonly used approach, is very sensitive to tube orientation). While several experimental results indicate that there is a distribution in the diameters of the nanotubes present in the samples, this observation does not by itself allow the conclusion that there is a heterogeneous distribution of tube diameters within individual bundles. Indeed, some of the structural studies[17] have modeled the experimental data by assuming that the samples are constituted by homogeneous bundles of tubes of different diameters and have justified this distribution on the physical grounds that tubes of different diameters are produced at different temperatures along the production stream.

Recently, an alternative thermodynamic approach has been suggested to resolve the questions of which of the models for the SWNT bundles more accurately describes them and where on the bundles is adsorption occurring. This approach is based on the fact that the geometrical arrangements of tubes present in the different bundle models result in distributions of adsorption energies that will be different for the different models.[11] Comparison of values obtained from experiments for the isosteric heat of adsorption with those obtained from computer simulations using the different theoretical models should allow the determination of which of the different models for the structure of the bundles describes them better.

Here, we compare experimental data obtained from argon adsorption isotherms measured over a wide range of tempera-

* Author to whom correspondence should be addressed. Phone: 618-453-1053. Fax: 618-453-1056. E-mail: aldo@physics.siu.edu.
[†] Department of Physics, Southern Illinois University.
[‡] Steacie Institute for Molecular Sciences, National Research Council.

10.1021/jp044266u CCC: $30.25
Published on Web 04/26/2005

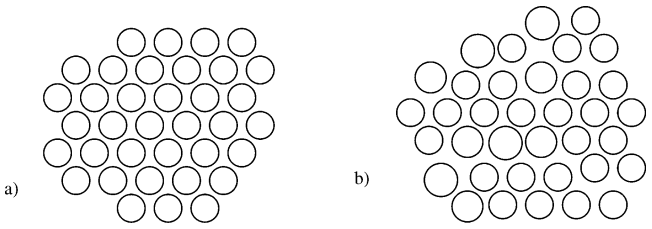

Figure 1. Schematic drawings of (a) homogeneous and (b) heterogeneous nanotube bundles.

tures and coverages, with theoretical simulation results for the coverage dependence of the isosteric heat for heterogeneous and homogeneous bundles. We also compare our results to those from prior experimental work on this system.

2. Experimental Section

The single-walled carbon nanotubes that we used as substrates were synthesized using a two-laser method.[21] Briefly, a rotating target composed of graphite, cobalt, and nickel was mounted at the center of a 45-mm quartz tube filled with a buffer of flowing argon gas (250 sccm, 500 Torr), all heated to a temperature of 1450 K by a split electric tube furnace. The first laser, which vaporized material from the target, was a Spectra-Physics Pro290-30 operating at a wavelength of 532 nm, a repetition rate of 30 Hz, and a fluence at the target of 1 J cm^{-2} $pulse^{-1}$. The second laser was a Spectra-Physics Tornado S240-TN50-106Q operating at 1064 nm with a pulse frequency of 20 kHz and average power of 48 W at the target. The role of this second laser was to interact with the plume of ejected material, altering the thermal gradient to promote a more efficient conversion of material into SWNTs as the plume cooled and condensed.[21] This second laser beam was expanded such that it encompassed the entire plume of material generated by the pulsed vaporization laser. The SWNTs were carried away from the hot zone of the furnace by the Ar gas, and they were deposited as a thick rubbery mat on a water-cooled collector.

Evaluation of the fraction of SWNTs contained in the sample was done using a combination of Raman spectroscopy, thermogravimetric analysis (TGA), and electron microscopy (see ref 21). The Raman spectrum and TGA data for the material used here are given in Figures 2a and 2b, respectively.

The Raman spectrum shows strong radial mode and G-band features and a weak disorder-induced D-band. The narrow radial mode peak at 180 cm^{-1} shift indicates a narrow diameter distribution with an average diameter of 1.33 nm based on the formula $\omega_{RBM}(cm^{-1}) = 223.5/d + 12.5$. (ref 22) This average diameter has been corroborated by direct TEM measurements.[21] From Figure 2b, the relative mass trace shows that greater than 90% of the mass is lost during the complete oxidation process, indicating that there is little metal catalyst in the sample. The differential mass trace highlights that the majority of material is lost during a single oxidation event occurring at a temperature of 375 °C. The primary contribution to this feature is the oxidation of SWNTs at lower than normal temperatures, induced by the exothermic oxidation of impurity carbons in contact with the SWNTs.[21] On the basis of the detailed analysis of the characterization data reported in ref 21, the estimated nanotube content in the sample used in this study is concluded to be approximately 60 wt %.

In our adsorption measurements, we used 0.134 g of sample without any post-production chemical treatment. The sample was outgassed in a quartz tube, under vacuum, to 250 °C for approximately 2 h and transferred, in air, to the experimental sample cell. A detailed description of the adsorption setup has been presented elsewhere.[23] We used Matheson Tri-Gas research purity Ar gas.

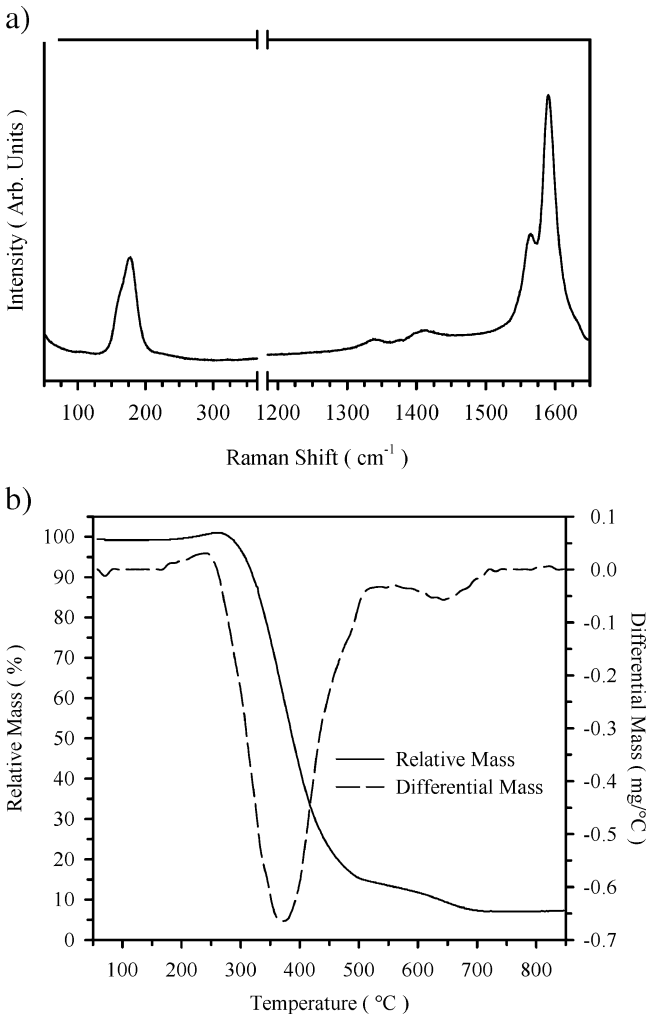

Figure 2. (a) Raman spectrum for the laser-grown SWNT sample studied here (excitation laser wavelength = 514 nm); (b) TGA data for the laser-grown SWNT sample studied here.

3. Results and Discussion

We measured isotherms at 21 temperatures ranging between 48 and 152 K (all these data are presented in Figure 3). Monolayer completion was determined using the point-B method.[24] For the sample used in these measurements, completion occurs around 4.29×10^{-4} mol (as determined from the isotherm measured at 81.933 K). The specific surface area of the sample was calculated assuming that the area per atom for Ar on the SWNTs is the same as that determined in the densest monolayer solid phase for Ar on planar graphite, 13.2 $Å^2$ $molecule^{-1}$.[6] We obtained a specific surface area of 253 m^2 g^{-1} for our sample.

The isosteric heat values were obtained from the adsorption isotherm data shown in Figure 3, using eq 1. Details of the calculations are described elsewhere.[25]

$$q_{st} = kT^2[\partial \ln(P)/\partial T]_\rho \quad (1)$$

None of the isotherms measured (Figure 3) spans the entire range of coverages needed for the determination of the isosteric heat as a function of coverage over the complete range studied here. Consequently, data from different temperature intervals were used to obtain the isosteric heats for different coverage ranges.

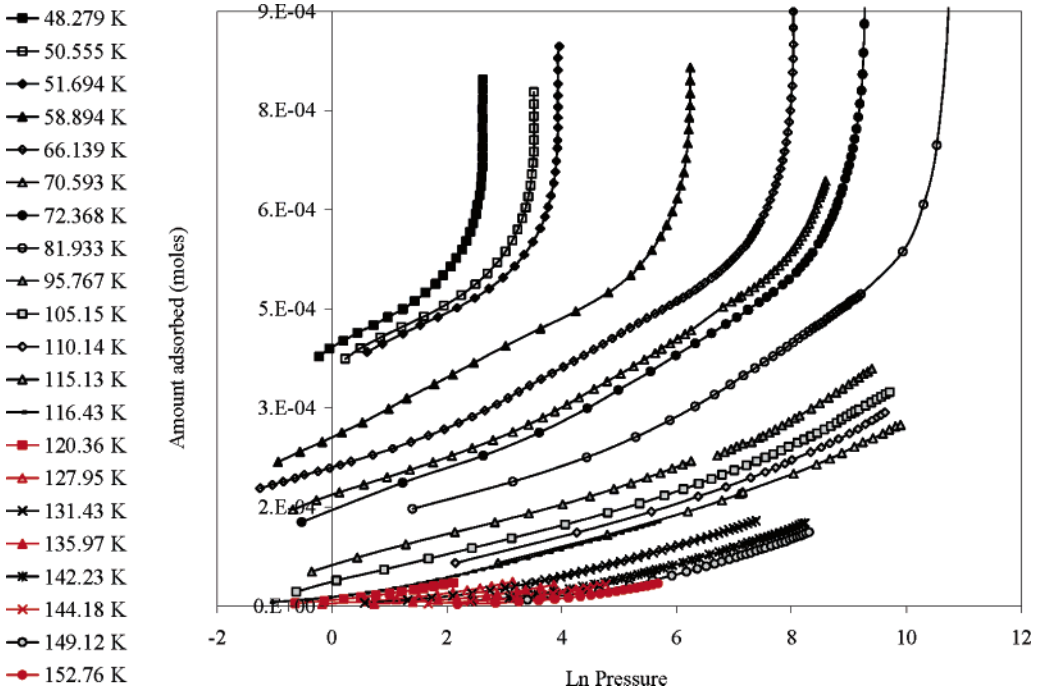

Figure 3. Argon adsorption isotherms.

TABLE 1: Information on Number of Isotherms Used for q_{st} Calculations in Different Coverage Ranges

coverage range ($\times 10^{-4}$ mol)	fractional coverage	temperature range (K)	no. of isotherms in that range
0.059 − 0.26	0.01−0.06	116.43−152.76	8
0.29 − 0.59	0.07−0.14	116.43−149.11	4
0.71−1.1	0.16−0.25	105.16−149.11	7
1.2−1.4	0.27−0.33	105.16−115.13	3
1.5−1.8	0.36−0.41	70.593−115.13	5
1.9−2.2	0.44−0.52	66.139−115.13	8
2.4−2.7	0.55−0.63	66.139−115.13	8
2.8−2.9	0.66−0.68	66.139−110.14	7
3.1−3.2	0.71−0.74	66.139−81.933	5
3.3−3.8	0.77−0.88	58.894−81.933	5
3.9−4.6	0.90−1.07	48.279−81.933	8
4.7−6.1	1.10−1.42	48.279−72.368	7
6.2−6.5	1.45−1.51	51.694−72.368	6

TABLE 2: Isosteric Heat Values

coverage ($\times 10^{-4}$ mol)	fractional coverage	average q_{st} (meV)
0.059	0.01	186
0.59	0.14	171
1.2	0.27	147
1.8	0.41	116
2.4	0.55	108
2.9	0.68	102
3.5	0.81	98
4.1	0.95	82
4.7	1.10	78
5.3	1.24	78
5.9	1.38	79
6.5	1.51	79

The grid of temperatures and coverages used for the q_{st} calculations is provided in Table 1.

The values of the isosteric heat corresponding to a given coverage were calculated as the average value obtained for this quantity by calculating the isosteric heat for every pair of temperatures for which there was isotherm data available in the given coverage range (Table 1). These values are presented in Table 2. The large number of temperatures used and the small coverage intervals between data points at each temperature permit a very careful determination of the coverage dependence of the isosteric heat starting from zero coverage and ending in the second layer.

The results presented in Table 2 for the isosteric heat are consistent with the ones that this group measured for argon adsorbed on a sample of SWNTs of lower purity produced by the arc-discharge method.[26] At the lowest coverage explored, the values of the isosteric heat reported in the previous study are higher than those reported here by about 5%. Another experimental exploration of Ar on arc-discharge-produced nanotubes[8] obtained isosteric heat values around 160 meV at the lowest coverages, also consistent with the results obtained here in this regime.

The values of the low coverage isosteric heat can be used to determine the binding energy of the Ar atoms to the strongest binding sites available on the nanotube substrate (see refs 5 and 26). Using this procedure, we obtain a value of 163 meV on these sites. This value is 65% higher than that for Ar adsorbed on planar graphite. The increase in the value of the binding energy on the nanotubes relative to that measured on planar graphite is in good agreement with values from other reports for Ar (and for other simple adsorbates) for this quantity.

In Figure 4, we compare our experimental results for the isosteric heat of adsorption as a function of the fractional coverage to the values for this same quantity obtained from two different sets of computer simulations. The simulations are for Ar on two different nanotube bundle models: homogeneous bundles and heterogeneous bundles. (Unfortunately, there is no similar data available for the heterogeneous deformable model against which to contrast our results.) Both of the simulated bundles consist of 45 tubes; for the homogeneous bundle, all of the tubes are of the same diameter while for the heterogeneous bundle the tubes are of different diameters and there are large ICs present.[11]

As can be seen in Figure 4, in all cases the isosteric heat values decrease with increasing coverage. This is characteristic of a large number of simple atomic and molecular adsorbates that are strongly attracted by the SWNTs. Even though the results of the two simulations are similar, there are some important differences between them, especially at low coverages.

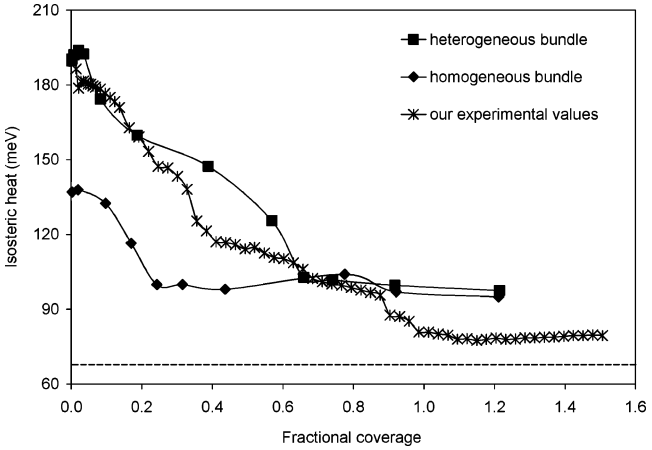

Figure 4. q_{st} coverage dependence; comparison of experimental and theoretical results. For reference, the value of the bulk heat of vaporization of Ar is given by the dashed horizontal line at 67 meV.

The highest values of the isosteric heat obtained in the two models differ by about 55 meV, or roughly $^1/_3$ of the total value, at the lowest coverages. The experimental value of the isosteric heat in this region is around 180 meV, closer to the 195 meV value for the heterogeneous bundle than to the homogeneous bundle's 140 meV. The higher-energy binding sites present in the heterogeneous model are the result of the small number of defect-induced, large-diameter interstitial channels that are readily accessible to the Ar atoms. These defect-induced sites are absent in the homogeneous bundle model, and consequently the highest-binding-energy sites for that defect-free structure are the grooves, which have a lower-binding-energy value.

It is clear that experimental isosteric heat data for Ar are in better agreement with the heterogeneous bundle model.

While the agreement between experimental and simulated isosteric heats constitutes a strong argument in favor of the structure for the bundles on which the heterogeneous model is based and in favor of Ar adsorption occurring in the defect-induced, large-diameter ICs present in this model, we note that there remain other aspects that need to be explored further. Previous surface area measurements conducted on a sample of as-produced HiPco nanotubes obtained using different adsorbates (Ne, Ar, CH_4, and Xe) yield specific area values that are very close to one another.[6] This experimental result indicates that the same sites are available to these different adsorbate species. The simulations with the heterogeneous model should be able to reproduce this result as well, if this model provides the correct description for the bundles.

Additionally, preliminary results for the coverage dependence of the isosteric heat of Xe on HiPco nanotubes[27] exhibit a somewhat lower level of agreement between the experiments and the simulations than that observed in this case for Ar. It is possible that these differences are the results of actual differences in the bundles that result when nanotubes are prepared by different procedures (i.e., that different methods produce tubes of different diameters), but it is also possible that there may be other origins for this difference.

Two possibilities that, to our knowledge, have not yet been explored in the simulations, but that could yield a small number of high-energy sites include the following: the possibility that the bundles are homogeneous, but that different bundles are made of tubes of different diameters (different diameter tubes will have different values for the binding energy in the grooves); or the possibility that a small fraction of the tubes are open ended, resulting in some high-energy binding sites inside the tubes. It would be interesting to have computer simulations for these scenarios to provide a more complete comparison between simulations and experiments.

4. Conclusions

We have determined the coverage dependence of the isosteric heat of adsorption for argon on SWNTs prepared by laser ablation. We compared our data with computer simulation results obtained from two different models for the bundles (homogeneous and heterogeneous). We found that our isosteric heat results are in better agreement with those from the heterogeneous bundle model.

Acknowledgment. A.D.M. acknowledges the National Science Foundation for support through Grant No. DMR-0089713. We acknowledge helpful discussions with J. K. Johnson and W. Shi.

References and Notes

(1) Iijima, S.; Ichihashi, T. *Nature* **1993**, *363*, 603.

(2) Thess, A.; Lee, R.; Nikolaev, P.; Dai, H. *Science* **1996**, *273*, 487.

(3) Stan, G.; Bojan, M. J.; Curtarolo, S.; Gatica, S. M.; Cole, M. W. *Phys. Rev. B* **2000**, *62*, 2173.

(4) Calbi, M. M.; Cole, M. W.; Gatica, S. M.; Bojan, M. J.; Stan, G. *Rev. Mod. Phys.* **2001**, *73*, 857.

(5) Talapatra, S.; Zambano, A. Z.; Weber, S. E.; Migone, A. D. *Phys. Rev. Lett.* **2000**, *85*, 138.

(6) Krungleviciute, V.; Heroux, L.; Talapatra, S.; Migone, A. D. *Nano Lett.* **2004**, *4*, 1133.

(7) Muris, M.; Dupont-Pavlovsky, N.; Bienfait, M.; Zeppenfeld, P. *Surf. Sci.* **2001**, *492*, 67.

(8) Wilson, T.; Tyburski, A.; DePies, M. R.; Vilches, O. E.; Becquet, D.; Bienfait, M. *J. Low Temp. Phys.* **2002**, *126*, 403.

(9) Wilson, T.; Vilches, O. E. *Physica B* **2003**, *329*−*333*, 278.

(10) Fujiwara, A.; Ishii, K.; Suematsu, H.; Kataura, H. et al. *Chem. Phys. Lett.* **2001**, *336*, 205.

(11) Shi, W.; Johnson, J. K. *Phys. Rev. Lett.* **2003**, *91*, 015504.

(12) Johnson, M. R.; Rols, S.; Wass, P.; Muris, M.; Bienfait, M.; Zeppenfeld, P.; Dupont-Pavlovsky, N. *Chem. Phys.* **2003**, *293*, 217.

(13) Rao, A. M.; Richter, E.; Bandow, S.; Chase, B. et al. *Science* **1997**, *275*, 187.

(14) Rinzler, A. G.; Liu, J.; Dai, H.; Nikolaev, P. et al. *Appl. Phys. A* **1998**, *67*, 29.

(15) Bandow, S.; Asaka, S.; Saito, Y.; Rao, A. M. *Phys. Rev. Lett.* **1998**, *80*, 3779.

(16) Lambin, Ph.; Loiseau, A.; Culot, C.; Biro, L. P. *Carbon* **2002**, *40*, 1635.

(17) Rols. S.; Almairac, R.; Henrard, L.; Anglaret, E. *Eur. Phys. J. B* **1999**, *10*, 263.

(18) Rols, S.; Righi, A.; Alvarez, L.; Anglaret, E. *Eur. Phys. J. B* **2000**, *18*, 201.

(19) Liu, J.; Rinzler, A. G.; Dai, H.; Hafner, J. H. et al. *Science* **1998**, *280*, 1253.

(20) Wildoer, J. W. G.; Venema, L. C.; Rinzler, A. G.; Smalley, R. E. *Nature* **1998**, *391*, 5962.

(21) Kingston, C. T.; Jakubek, Z. J.; Denommee, S.; Simard, B. *Carbon* **2004**, *42*, 1657.

(22) Bachilo, S. M.; Strano, M. S.; Kittrell, C.; Hauge, R. H. et al. *Science* **2002**, *298*, 2361.

(23) Shrestha, P.; Alkhafaji, M. T.; Lukowitz, M. M. et al. *Langmuir* **1994**, *10*, 3244.

(24) Gregg, S. J.; Sing, K. S. W. *Adsorption, Surface Area and Porosity*; Academic Press: London, 1967; pp 54−56.

(25) Weber, S. E.; Talapatra, S.; Journet, C.; Zambano, A. *Phys. Rev. B* **2000**, *61*, 13150.

(26) Talapatra, S.; Rawat, D. S.; Migone, A. D. *J. Nanosci. Nanotechnol.* **2002**, *2*, 467.

(27) Rawat, D. S.; Krungleviciute, V.; Migone A. D. Unpublished work.